

Real-space imaging of kagome flat band localization in Fe_3Sn_2

Yifan Wang(汪逸凡), Lili Jiang(蒋利利), Qiang Zhang(张强), Zhiyong Lin(林志勇), Hui Zhang(张汇), and Changgan Zeng(曾长淦)

Citation: Chin. Phys. B, 2026, 35 (**3**): 036801. DOI: 10.1088/1674-1056/ae2f53
http://cpb.iphy.ac.cn; http://iopscience.iop.org/cpb

What follows is a list of articles you may be interested in

Bond-resolved silicene on Au(111) substrate

Ye Chen(陈烨), Wenya Zhai(翟文雅), Haoyuan Zang(臧浩原), Zengfu Ou(欧增福), Donghui Guo(郭东辉), and Jingcheng Li(李竟成)

Chin. Phys. B, 2025, 34 (**9**): 096801. DOI: 10.1088/1674-1056/adee02

Characterization of antisite defects and in-gap states in antiferromagnetic $MnSb_2Te_4$

Junming Zhang(张峻铭), Ming Xi(席明), Yuchong Zhang(张羽翀), Hang Li(李航), Jiali Zhao(赵佳丽), Hechang Lei(雷和畅), Zhongxu Wei(魏忠旭), and Tian Qian(钱天)

Chin. Phys. B, 2025, 34 (**7**): 076801. DOI: 10.1088/1674-1056/adcea3

Surface solitonic charge distribution on 2D materials investigated using Kelvin probe force microscopy technique based on qplus atomic force microscopy

Rui Song(宋睿), Feng Hao(郝峰), Jie Yang(杨杰), Lifeng Yin(殷立峰), and Jian Shen(沈健)

Chin. Phys. B, 2025, 34 (**5**): 056802. DOI: 10.1088/1674-1056/adbee8

Emergent 3×3 charge order on the Cs reconstruction of kagome superconductor CsV_3Sb_5

Xianghe Han(韩相和), Zhongyi Cao(曹钟一), Zihao Huang(黄子豪), Zhen Zhao(赵振), Haitao Yang(杨海涛), Hui Chen(陈辉), and Hong-Jun Gao(高鸿钧)

Chin. Phys. B, 2025, 34 (**1**): 016801. DOI: 10.1088/1674-1056/ad8fa1

Surface evolution of thermoelectric material KCu_4Se_3 explored by scanning tunneling microscopy

Yumin Xia(夏玉敏), Ni Ma(马妮), Desheng Cai(蔡德胜), Yuzhou Liu(刘宇舟), Yitong Gu(谷易通), Gan Yu(于淦), Siyu Huo(霍思宇), Wenhui Pang(庞文慧), Chong Xiao(肖翀), and Shengyong Qin(秦胜勇)

Chin. Phys. B, 2024, 33 (**8**): 086804. DOI: 10.1088/1674-1056/ad50c4

RAPID COMMUNICATION

Real-space imaging of kagome flat band localization in Fe_3Sn_2

Yifan Wang(汪逸凡)[1,2,3], Lili Jiang(蒋利利)[1,2,3], Qiang Zhang(张强)[1,2,3], Zhiyong Lin(林志勇)[1,2,3], Hui Zhang(张汇)[1,2,3,†], and Changgan Zeng(曾长淦)[1,2,3,‡]

[1] *CAS Key Laboratory of Strongly-Coupled Quantum Matter Physics, and Department of Physics, University of Science and Technology of China, Hefei* 230026, *China*

[2] *International Center for Quantum Design of Functional Materials (ICQD), Hefei National Research Center for Physical Sciences at the Microscale, University of Science and Technology of China, Hefei* 230026, *China*

[3] *Hefei National Laboratory, University of Science and Technology of China, Hefei* 230088, *China*

(Received 29 September 2025; revised manuscript received 12 December 2025; accepted manuscript online 19 December 2025)

In geometrically frustrated lattices, flat bands can arise from destructive quantum interference, providing an ideal platform for exploring strong electron correlations. However, direct real-space evidence of their predicted atomic-scale electron localization remains elusive. By employing scanning tunneling microscopy/spectroscopy, with a focus on quasiparticle interference imaging, we demonstrate unambiguous atomic-scale localization of flat band electrons in the kagome metal Fe_3Sn_2. Crucially, quasiparticle interference imaging reveals a complete suppression of scattering wavevectors and standing waves exclusively at the flat band energy, indicating the absence of long-range coherent propagation. This disappearance of the quasiparticle interference signal, attributable to the non-propagating wavefunctions inherent to the kagome flat band, directly confirms real-space electron localization. These findings resolve the microscopic link between quantum interference and localization of flat band electrons, paving the way for engineering correlated quantum states.

Keywords: scanning tunneling microscopy, kagome, flat band, electron localization, quasiparticle interference

PACS: 68.37.–d, 68.37.Ef, 71.20.–b, 73.20.At

DOI: 10.1088/1674-1056/ae2f53 **CSTR:** 32038.14.CPB.ae2f53

Flat band represents a unique electronic band structure characterized by constant energy across the crystal momentum space.[1–7] A defining feature of flat band is that charge carriers within them exhibit vanishing group velocity and divergent effective mass, resulting in quenched kinetic energy and an extraordinarily high density of states. These distinctive properties establish flat bands as a unique and powerful platform for investigating strongly correlated quantum phenomena. These effects include ferromagnetism,[8] superconductivity,[9–12] Wigner crystallization,[13] high-temperature fractional quantum Hall states,[14–17] and Bose–Einstein condensation.[18] Their emergence stems from the quenched kinetic energy of the carriers in flat bands, which allows Coulomb interactions to dominate. Notable examples of systems that host such flat bands include the dice lattice,[19] Lieb lattice,[20] kagome lattice,[21–23] and Tasaki lattice.[3] Particularly in the kagome lattice, which consists of interlaced triangles with each lattice site connecting two neighboring hexagons, the alternating sign of electron wave functions at the six vertices of each hexagon leads to destructive interference outside the hexagon. This constitutes the fundamental mechanism enabling flat bands, as it forces electrons to localize and circulate around each hexagonal ring (Fig. 1(a)).

To date, experimental observations have revealed flat bands via angle-resolved photoemission spectroscopy (ARPES) in a range of kagome crystals, such as CoSn,[24,25] $Co_3Sn_2S_2$,[26] FeSn,[27,28] and Fe_3Sn_2.[29–32] Critically, the intrinsic properties of flat bands suppress electron kinetic energy relative to Coulomb repulsion, promoting localization wherein electrons are confined to specific lattice sites rather than being delocalized freely. However, the direct and unambiguous characterization of this electron localization phenomenon induced by the intrinsic nature of flat bands in real space has remained elusive. In this work, we leverage quasiparticle interference (QPI) by scanning tunneling microscopy (STM) to systematically probe the electronic localization behavior within the kagome-derived flat band of Fe_3Sn_2.

QPI is a fundamental quantum phenomenon arising from the elastic scattering of quasiparticles by atomic-scale defects or impurities in condensed matter systems.[33–35] Its physical mechanism involves the coherent superposition of incident and scattered electron waves, generating spatially periodic oscillations in the local density of states (LDOS). These spatial oscillations, known as Friedel oscillations, reflect interference patterns between incident and scattered electron waves. In 2D systems, QPI serves as a powerful probe for electronic properties such as band structure,[36] Fermi surface topology,[37] chirality,[38] and spin–valley coupling.[39] Fourier transform

†Corresponding author. E-mail: huiz@ustc.edu.cn

‡Corresponding author. E-mail: cgzeng@ustc.edu.cn

© 2026 Chinese Physical Society and IOP Publishing Ltd. All rights, including for text and data mining, AI training, and similar technologies, are reserved.

(FT) in STM/STS is the key technique for visualizing QPI. By performing a 2D FT on real-space LDOS maps, scattering wave vectors in reciprocal space are resolved. These vectors connect points on constant energy contours of the band structure, revealing allowed scattering channels. Therefore, QPI serves as a definitive fingerprint of electron delocalization.

Basic structural and electronic characterizations of Fe_3Sn_2 are shown in Fig. 1. The Fe_3Sn_2 compound possesses a rhombohedral crystal structure with two adjacent Fe–Sn layers separated by a Sn honeycomb layer (Fig. 1(a)). Intermittent interfacial configurations of Fe–Sn and Sn terminations intersecting at half-unit-cell step edges (Fig. 1(b)) exhibit a measured step height of 0.2 nm in the STM topographic profile, which is consistent with the crystallographic dimensions. Atomic-resolution STM images acquired at −0.2 eV across distinct layers (Fig. 1(b)) enable clear differentiation between the Sn layer and the Fe–Sn kagome layer. These structural features are consistent with those reported in a previous study.[29]

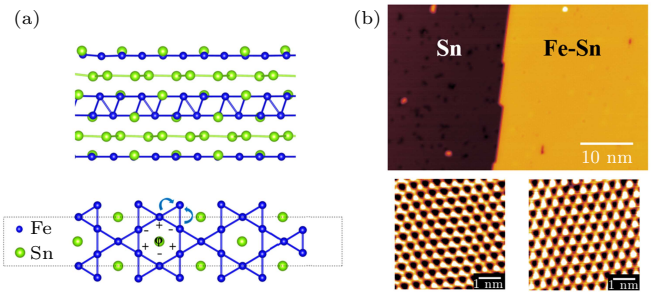


Fig. 1. (a) Side and top views of the optimized structure of bulk Fe_3Sn_2. Schematic diagram of the wave function self-localization due to the destructive interference on the hexagons in the kagome lattice. (b) (Top) Topographic image of a cleaved Fe_3Sn_2 surface revealing two distinct surface layers ($V_s = 0.5$ eV, $I_t = 500$ pA). (Bottom) Atomic resolution STM images of the two different surface layers acquired at −0.2 eV, showing the Sn layer (left) and the Fe–Sn kagome layer (right).

ARPES measurements of Fe_3Sn_2 reveal a distinct nearly dispersionless flat band localized near −0.2 eV (Fig. 2(a)). On the other hand, dI/dV spectra were obtained away from defects for both the Fe–Sn layer and the Sn layer (Fig. 2(b)). Crucially, the Fe–Sn layer (blue curve) exhibits a pronounced peak at −0.2 eV resulting from the flat band formed by the Fe kagome lattice, while the Sn layer (red curve) shows no such feature due to its non-kagome structure. The dI/dV map of the Fe–Sn layer at −0.2 eV (Fig. 2(c)) exhibits a well-defined electronic kagome lattice signature. For comparison, the dI/dV maps acquired at −0.1 eV and −0.35 eV are presented in Fig. 2(d), in which no electronic kagome lattice signature is observed. These experimental observations indicate that the kagome geometry of the Fe–Sn layers is the primary origin of the flat band.

Subsequently, QPI investigations were performed on the Fe–Sn layer. By analyzing small-scale dI/dV maps acquired at varying energies, pronounced energy-dependent variations in interference patterns were observed near the defects. Specifically, at −0.05 eV, −0.1 eV, and −0.35 eV (Figs. 3(a), 3(b), and 3(d), respectively), distinct standing wave modulations emerge around defects, indicating coherent quasiparticle scattering. In sharp contrast, such interference patterns are strongly suppressed at −0.2 eV (Fig. 3(c)), i.e., at the flat band energy. The observed energy-dependent electron scattering can be explained as follows. Away from the flat band, the free propagation of electrons enables interference near defects and leads to the formation of standing wave patterns. At the flat band energy of −0.2 eV, on the contrary, electrons become spatially localized due to their non-propagating wavefunctions, which prevents long-range coherent scattering and therefore suppresses standing waves. Consequently, the absence of interference at −0.2 eV provides direct evidence for flat-band electron localization.

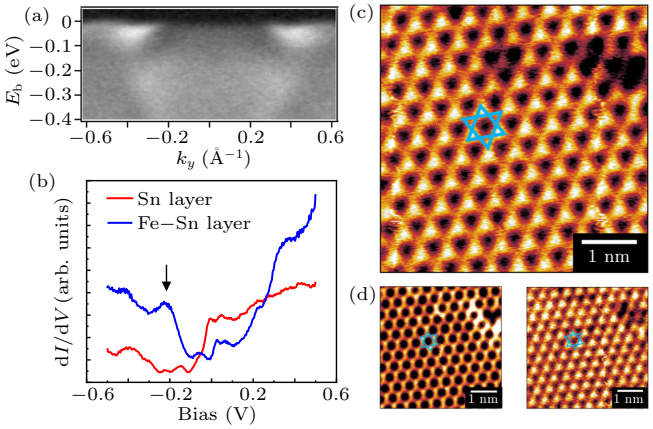


Fig. 2. Band dispersion of Fe_3Sn_2 along the Γ–K lines by ARPES. (b) dI/dV spectra obtained on Sn layer and Fe–Sn layer, respectively. The black arrow indicates the flat band at −0.2 eV. (c) dI/dV map taken at −0.2 eV on Fe–Sn layer, showing electronic states localized to the kagome lattice ($I_t = 300$ pA). The blue lines denote the kagome lattice. (d) dI/dV maps taken at −0.1 eV (left) and −0.35 eV (right), respectively, showing a striking contrast with the −0.2 eV map. The blue lines denote the kagome lattice.

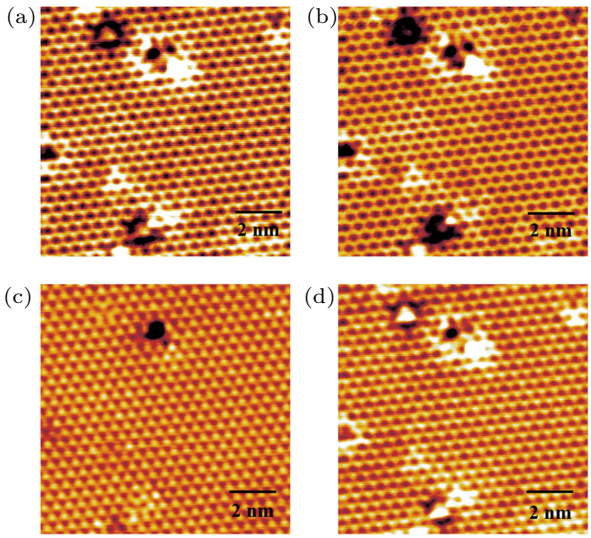


Fig. 3. (a)–(d) dI/dV map near the defects taken at −0.05 eV, −0.1 eV, −0.2 eV and −0.35 eV, respectively ($I_t = 400$ pA), showing a striking contrast with the −0.2 eV map.

For comprehensive momentum-space characterization of

the scattering wavevectors, we acquired large-scale $\mathrm{d}I/\mathrm{d}V$ maps of the Fe–Sn layer at multiple bias voltages (Figs. 4(a)–4(c), top panels) and obtained their FT power spectra (Figs. 4(a)–4(c), bottom panels). The direction and intensity of the prominent wavevectors in close proximity to the central region of the FT power spectrum were measured. The wavevector $\boldsymbol{q}_{\mathrm{Bragg}}$ corresponds to the atomic Bragg peaks related to the *ab*-plane lattice vectors and is circled in red. At the energy of −0.05 eV and −0.35 eV, we identified a symmetric signal marked by yellow circles, which corresponds to the wavevector $\boldsymbol{q}$ of the dominating electron scattering at the corresponding energy (Figs. 4(a) and 4(c)). Based on the direction and magnitude of the Bragg peaks, it can be inferred that the scattering wavevector matches the direction of the $\boldsymbol{q}_{\mathrm{Bragg}}$, with a wavevector magnitude of 0.8 $\mathrm{Å}^{-1}$ and 0.6 $\mathrm{Å}^{-1}$, respectively. This is consistent with the value of the Fermi wavevector observed in the constant-energy contour of our ARPES experiment at the corresponding energy. In sharp contrast, upon the energy shift to −0.2 eV, $\boldsymbol{q}$ completely vanishes, leaving only the presence of diffuse scattering wavevectors predominantly concentrated near the central region of the FT power spectrum. (Figs. 4(b)). Figure 4(d) shows the line cuts of different energies generated from the FT power spectrum along the direction of $\boldsymbol{q}$. Complete suppression of the wavevector $\boldsymbol{q}$ is observed at a flat band energy of −0.2 eV. However, the wavevector $\boldsymbol{q}$ can be observed at other energies.

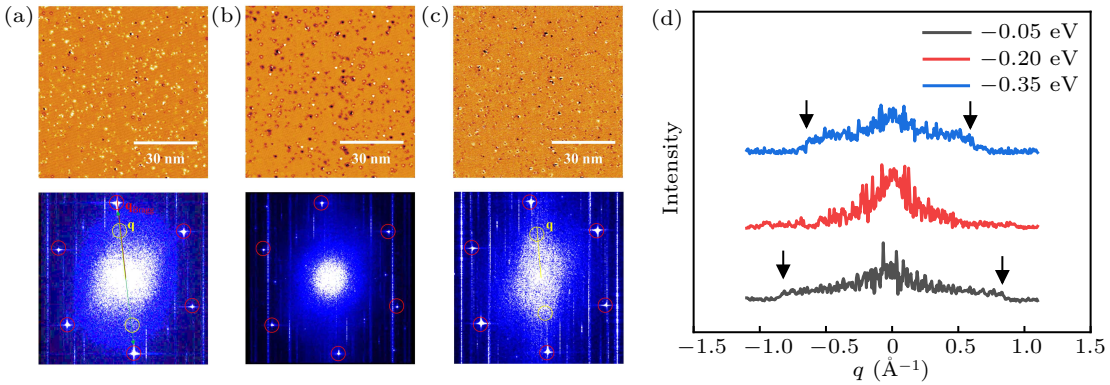


Fig. 4. (a)–(c) (Top) $\mathrm{d}I/\mathrm{d}V$ maps captured on the Fe–Sn layer at −0.05 eV, −0.2 eV and −0.35 eV, respectively ($I_{\mathrm{t}} = 300$ pA). (Bottom) FT power spectra at corresponding energies. The wavevectors of the lattice $\boldsymbol{q}_{\mathrm{Bragg}}$ are encircled in red and the scattering wavevector $\boldsymbol{q}$ is encircled in yellow. (d) Normalized radial average line-cuts derived from the FT power spectra along the wavevector $\boldsymbol{q}$ marked by the green line in (a)–(c) at corresponding energies with the black arrows mark the approximate positions of the QPI signals.

In summary, our QPI imaging experiments provide direct evidence of a complete suppression of the scattering electron wavevectors at the flat band energy, confirming the spatial localization of flat band electrons. This absence of QPI signatures originates from the non-propagating nature of localized electrons. These findings lay a foundation for exploring correlated phenomena in localized flat-band systems. On the other hand, the QPI methodology adopted in this work provides a universal framework to identify atomic-scale flat band localization.

Data availability statement

The data that support the findings of this study are openly available in Science Data Bank at https://doi.org/10.57760/sciencedb.j00113.00288.

Acknowledgements

This work was supported by the National Key Research and Development Program of China (Grant No. 2023YFA1406300), the Innovation Program for Quantum Science and Technology (Grant No. 2021ZD0302800), the National Natural Science Foundation of China (Grant Nos. 92165201, 12374458, 12488101, and 11974323), Anhui Provincial Key Research and Development Project (Grant No. 2023z04020008), the CAS Project for Young Scientists in Basic Research (Grant No. YSBR-046), the Fundamental Research Funds for the Central Universities (Grant No. WK9990000118), and the Strategic Priority Research Program of Chinese Academy of Sciences (Grant No. XDB0510200).

References

[1] Mielke A 1991 *J. Phys. A* **24** 3311
[2] Mielke A 1991 *J. Phys. A* **24** L73
[3] Tasaki H 1992 *Phys. Rev. Lett.* **69** 1608
[4] Tasaki H 1998 *Prog. Theor. Phys.* **99** 489
[5] Tsui D C, Stormer H L and Gossard A C 1982 *Phys. Rev. Lett.* **48** 1559
[6] Laughlin R B 1983 *Phys. Rev. Lett.* **50** 1395
[7] Si Q and Steglich F 2010 *Science* **329** 1161
[8] Hase I, Yanagisawa T, Aiura Y and Kawashima K 2018 *Phys. Rev. Lett.* **120** 196401
[9] Yankowitz M, Chen S, Polshyn H, Zhang Y, Watanabe K, Taniguchi T, Graf D, Young A F and Dean C R 2019 *Science* **363** 1059
[10] Kopnin N B, Heikkilä T T and Volovik G E 2011 *Phys. Rev. B* **83** 220503
[11] Imada M and Kohno M 2000 *Phys. Rev. Lett.* **84** 143
[12] Peotta S and Törmä P 2015 *Nat. Commun.* **6** 8944
[13] Wu C, Bergman D, Balents L and Das Sarma S 2007 *Phys. Rev. Lett.* **99** 070401

[14] Tang E, Mei J and Wen X 2011 *Phys. Rev. Lett.* **106** 236802

[15] Sun K, Gu Z, Katsura H and Das Sarma S 2011 *Phys. Rev. Lett.* **106** 236803

[16] Neupert T, Santos L, Chamon C and Mudry C 2011 *Phys. Rev. Lett.* **106** 236804

[17] Wang Y, Gu Z, Gong C and Sheng D 2011 *Phys. Rev. Lett.* **107** 146803

[18] Huber S D and Altman E 2010 *Phys. Rev. B* **82** 184502

[19] Sutherland B 1986 *Phys. Rev. B* **34** 5208

[20] Lieb E H 1989 *Phys. Rev. Lett.* **62** 1201

[21] Huhtinen K E, Tylutki M, Kumar P, Vanhala T I, Peotta S and Törmä P 2018 *Phys. Rev. B* **97** 214503

[22] Li Z, Zhuang J, Wang L, Feng H, Gao Q, Xu X, Hao W, Wang X, Zhang C, Wu K, Dou S X, Chen L, Hu Z and Du Y 2018 *Sci. Adv.* **4** 4511

[23] Mielke A 1992 *J. Phys. A* **25** 4335

[24] Kang M, Fang S, Ye L, Po H C, Denlinger J, Jozwiak C, Bostwick A, Rotenberg E, Kaxiras E, Checkelsky J and Comin R 2020 *Nat. Commun.* **11** 4004

[25] Liu Z, Li M, Wang Q, Wang G, Wen C, Jiang K, Lu X, Yan S, Huang Y, Shen D, Yin J, Wang Z, Yin Z, Lei H and Wang S 2020 *Nat. Commun.* **11** 4002

[26] Yin J, Zhang S, Chang G, Wang Q, Tsirkin S, Guguchia Z, Lian B, Zhou H, Jiang K, Belopolski I, Shumiya N, Multer D, Litskevich M, Cochran T, Lin H, Wang Z, Neupert T, Jia S, Lei H and Hasan M 2019 *Nat. Phys.* **15** 443

[27] Kang M, Ye L, Fang S, You J, Levitan A, Han M, Facio J, Jozwiak C, BostwickA, Rotenberg E, Chan M, McDonald R, Graf D, Kaznatcheev K, Vescovo E, Bell D, Kaxiras E, Brink J, Richter M, Ghimire M, Checkelsky J and Comin R 2020 *Nat. Mater.* **19** 163

[28] Lin Z, Wang C, Wang P, Yi S, Li L, Zhang Q, Wang Y, Wang Z, Huang H, Sun Y, Huang Y, Shen D, Feng D, Sun Z, Cho J, Zeng C and Zhang Z 2020 *Phys. Rev. B* **102** 155103

[29] Lin Z, Choi J, Zhang Q, Qin W, Yi S, Wang P, Li L, Wang Y, Zhang H, Sun Z, Wei L, Zhang S, Guo T, Lu Q, Cho J, Zeng C and Zhang Z 2018 *Phys. Rev. Lett.* **121** 096401

[30] Yin J, Zhang S, Li H, Jiang K, Chang G, Zhang B, Lian B, Xiang C, Belopolski I, Zheng H, Cochran T, Xu S, Bian G, Liu K, Chang T, Lin H, Lu Z, Wang Z, Jia S, Wang W and Hasan M 2018 *Nature* **562** 91

[31] Lisi S, Lu X, Benschop T, Jong T, Stepanov P, Duran J, Margot F, Cucchi I, Cappelli E, Hunter A, Tamai A, Kandyba V, Giampietri A, Barinov A, Jobst J, Stalman V, Leeuwenhoek M, Watanabe K, Taniguchi T, Rademaker L, Molen S, Allan M, Efetov D and Baumberger F 2021 *Nat. Phys.* **17** 189

[32] Ye L, Kang M, Liu J, Cube F, Wicker C, Suzuki T, Jozwiak C, Bostwick A, Rotenberg E, Bell D, Fu L, Comin R and Checkelsky J 2018 *Nature* **555** 638

[33] Hasegawa Y and Avouris P 1993 *Phys. Rev. Lett.* **71** 1071

[34] Crommie F, Lutz P and Eigler M 1993 *Nature* **363** 524

[35] Sprunger T, Petersen L, Plummer W, Laegsgaard E and Besenbacher F 1997 *Science* **275** 1764

[36] Mallet P, Brihuega I, Bose S, Ugeda M M, Gomez-Rodriguez J M, Kern K and Veuillen J Y 2008 *Phys. Rev. B* **86** 045444

[37] Liu H, Chen J, Yu H, Yang F, Jiao L, Liu G, Ho W, Gao C, Jia J, Yao W and Xie M 2015 *Nat. Commun.* **6** 8180

[38] Brihuega I, Mallet P, Bena C, Bose S, Michaelis C, Vitali L, Varchon F, Magaud L, Kern K and Veuillen J Y 2008 *Phys. Rev. Lett.* **101** 206802

[39] Yankowitz M, McKenzie D and LeRoy B J 2015 *Phys. Rev. Lett.* **115** 136803